Mechanics of photosynthesis assisted polymer strengthening

Kunhao Yu, Zhangzhengrong Feng, Haixu Du, Qiming Wang [*]

Sonny Astani Department of Civil and Environmental Engineering, University of Southern California, Los Angeles, CA 90089, United States

A B S T R A C T

Plant cells utilize photosynthesis to produce glucose that is delivered to selected locations to form stiff polysaccharides (e.g., chitin, chitosan, and cellulose), which strengthen the plant structures. Such a photosynthesis-assisted strengthening behavior in plants has rarely been imitated in synthetic material systems. We here propose a synthetic polymer system embedded with extracted plant chloroplasts, which allow for the photosynthesis-assisted mechanical strengthening of the polymer matrix. The strengthening mechanism relies on an additional crosslinking reaction between the photosynthesis-produced glucose and side groups within the polymer matrix. We develop a theoretical framework to model the photosynthesis-assisted strengthening behaviors of polymers. The glucose production of the embedded chloroplasts will be first modeled with a general photosynthesis theory, and the exportation of glucose to the polymer matrix is modeled with an enzyme-assisted mass transport theory. Next, a polymer strengthening network model with glucose molecules as additional crosslinkers is presented. Effects of the illumination period, the concentration of embedded chloroplasts, and the light intensity on the stiffness strengthening are studied. The theoretical results consistently agree with the experimental results of the photosynthesis-assisted polymer strengthening.

1. Introduction

Plants offer continuous sources of inspiration for the engineering endeavor. Engineering materials inspired by plants provide great promise for designing and optimizing material properties and functionalities, such as hydrophobicity (Barthlott et al., 2010; Tricinci et al., 2015; Zeiger et al., 2016), mechanical properties (Gan et al., 2019; Li and Wang, 2015b; Sehaqui et al., 2010), remodeling (Del Dottore et al., 2018), self-healing (Yu et al., 2020a,2019b), and shape-changing (Armon et al., 2011; Correa et al., 2015; Li and Wang, 2015a, b). Of particular interest is plants' strengthening behavior: Plant cells utilize photosynthesis to produce glucose that is delivered to selected locations to form stiff polysaccharides (e.g., chitin, chitosan, and cellulose), which strengthen the plant structures (**Fig. 1**a) (Barthelemy and Caraglio, 2007; Popper et al., 2011). For example, the stiffness of a young stem is typically in the order of kilopascal, while the stiffness of a mature trunk can reach as high as several gigapascals (Shah et al., 2017). Although such a photosynthesis-assisted strengthening behavior is the basis of plants' growth and remodeling, how to imitate such strengthening behavior in a synthetic material system remains largely elusive.

Here, we propose a synthetic polymer system embedded with extracted plant chloroplasts, which allow for the photosynthesis-assisted mechanical strengthening of the polymer matrix (**Fig. 1**b)(Yu et al., 2021). The strengthening mechanism relies on an additional crosslinking reaction between the photosynthesis-produced glucose and side groups within the polymer matrix, thus

---

forming a stiff region with additional crosslinks (Fig. 1b). This material system provides a unique platform for strengthening and remodeling engineering materials via the communication between synthetic polymers and natural photosynthesis processes, thus opening the door for the design of hybrid synthetic-living materials, for applications such as smart composites and soft robotics. Moreover, the photosynthesis-assisted strengthening can usually be delivered locally to achieve on-demand strengthening performance, or to impart graded stiffness with graded light intensity, which has been a longstanding challenge in traditional fabrication processes that require continuously switching materials during fabrication (Bartlett et al., 2015). Despite the great potential, the fundamental understanding of this class of hybrid synthetic-living materials with living chloroplasts has been left behind due to two key reasons. First, the underlying mechanism between the living chloroplasts and the synthetic polymer system hasn't been well understood. Although several biochemical models have been proposed to capture the photosynthesis behavior of plants (Farquhar et al., 1980; Zhu et al., 2013), there is no theoretical model to quantitatively understand the photosynthesis process of extracted chloroplasts within a polymer matrix. It remains elusive how photosynthesis-produced glucose molecules interact with the polymer network. It is also unclear how to mechanistically understand the effects of the concentration and photosynthesis conditions of embedded chloroplasts on the material strengthening behavior. Second, the understanding of strengthening networks based on additional crosslinking remains elusive. How the additional crosslinks affect the existing polymer networks remains unknown. How
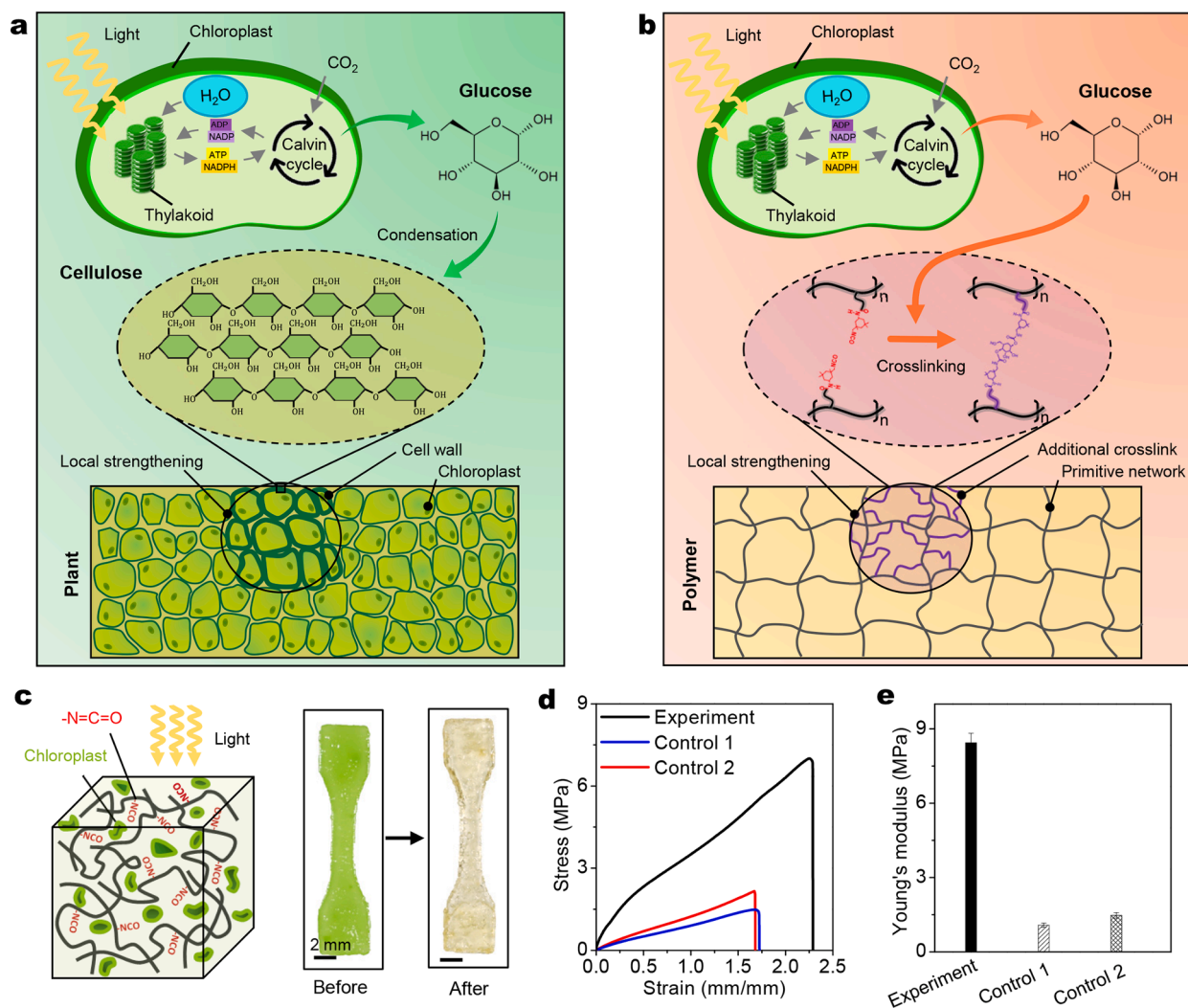

Fig. 1. (a) Schematics to illustrate photosynthesis-assisted remodeling of plants. The photosynthesis-produced glucose undergoes a condensation reaction to form stiff polysaccharides (e.g., cellulose). (b) Schematics to illustrate photosynthesis-assisted remodeling of a synthetic polymer. The photosynthesis-produced glucose undergoes a reaction with isocyanate (NCO) side groups to form additional crosslinks. (c) Schematic and sample with free NCO groups and embedded chloroplasts before and after undergoing 4-h light illumination and 4-h darkness. (d) Uniaxial tensile stress-strain curves of one experimental group and two control groups. The experimental group includes samples with free NCO groups and embedded chloroplasts undergoing 4-h light illumination and 4-h darkness. The control 1 group includes samples with free NCO groups and embedded chloroplasts undergoing 8-h darkness. The control 2 group includes samples with free NCO groups but without chloroplasts undergoing 4-h light illumination and 4-h darkness. (e) Young's moduli of three groups of samples.

the additional crosslinks affect the polymer chain evolution is also ambiguous. The missing of these aspects of theoretical understanding would significantly drag down the innovation of photosynthesis-assisted hybrid synthetic-living materials.

In this paper, we present a theoretical framework to model the self-strengthening behaviors of polymers assisted by the photosynthesis process. The strengthening mechanism of the synthetic polymer is shown in **Fig. 1b**. The photosynthesis-produced glucose can facilitate additional crosslinking reactions in the polymer matrix upon exposure to white light. The photosynthesis-assisted crosslinking is forming due to the reaction of open free isocyanate (NCO) groups in the material matrix and hydroxyl (OH) groups on the glucose, which enables the enhancement of mechanical properties of materials including Young's modulus and tensile strength (**Figs. 1c-e**). The photosynthesis-assisted glucose production of the embedded chloroplasts will be first modeled with a general photosynthesis theory. Then, the exportation of glucose from the chloroplasts to the polymer matrix is modeled with an enzyme-assisted mass transport theory. Next, the original polymer matrix is modeled with a network model with homogeneous chain length distribution. When the photosynthesis-produced glucose is introduced in the polymer matrix and form the additional crosslinks, inhomogeneous chain lengths are considered following two different algorithms. The formation of additional crosslinks will be examined by the comparison between experimental and theoretical results. Effects of the illumination period, the concentration of embedded chloroplasts, and the light intensity on the stiffness strengthening will be studied. The theoretical model can consistently explain experimentally observed photosynthesis-assisted strengthening.

The plan of the paper is as follows. **Section 2** introduces the experiments about the photosynthesis-assisted strengthening of a chloroplast-embedded polymer system. In **Section 3**, we present the theoretical model system by first considering the general theory for the photosynthesis process in the material matrix, then the model for polymer strengthening by additional crosslinking. In **Section 4**, we present the theoretical results from the photosynthesis model and then from the polymer strengthening model. With respective experiments and theories, the effects of the illumination period, the concentration of embedded chloroplasts, and the light intensity will be studied. The concluding remarks will be presented in **Section 5**.

2. Experimental

The polymer was prepared by embedding the extracted chloroplasts in a synthetic polymer matrix. The polymer with free NCO groups was prepared by preheating 0.01 mole of Poly(tetrahydrofuran) (PolyTHF, average molar mass 650 g/mol) at 100 °C, and exposed to the nitrogen environment for 1 h to remove moisture and oxygen. 0.02 mole of isophorone diisocyanate (IPDI), 10 wt% of dimethylacetamide (DMAc), and 1 wt% of dibutyltin dilaurate (DBTDL) were mixed with the preheated PolyTHF at 70 °C, and stirred with a magnetic stir bar for 1 h. After reducing the temperature to 40 °C, 0.01 mole of 2-Hydroxyethyl methacrylate (HEMA) was added and mixed for 1 h to complete the synthesis (0.02 mole of HEMA was added for the polymer without free NCO groups). Then, we extracted living chloroplasts from spinach leaves (Joly and Carpentier, 2011). The HEPES buffer solution was prepared by mixing HEPES buffer (30×10^{-3}M, pH 5.0–6.0), poly(ethylene glycol) (Mw. 8000, 10% (w/v)), $MgCl_2$ (2.5×10^{-3} M), K_3PO_4 (0.5×10^{-3} M), and DI Water. The HEPES buffer solution was then magnetically stirred for 3 h. NaOH solution was added to adjust the pH value to be around 7.6. The HEPES buffer solution was then stored in the fridge at 4 °C for 3 h before use. Then, the fresh baby spinach leaves (Spinacia oleracea L.) were washed with DI water and then dried to remove the surface water. Next, the middle veins of the leaves were removed to obtain 65 g leaf meat from about 100 g of fresh leaves. Then, the leaf meat was ground with 100 ml HEPES buffer solution in the pre-chilled kitchen blender for about 2 min until the mixture became homogeneous. The mixture was centrifuged with 4000 RPM for 15 min at 4 °C (Eppendorf 5804R). Then, the supernatant was removed, and the chloroplast pellet was re-suspended in the HEPES buffer solution. After adding the suspended mixture on the top of 5 mL of 40% Percoll in two pre-chilled tubes, we centrifuged the mixture at 3636 RPM for 8 min at 4 °C. Later, we removed the supernatant and kept the pellet. Next, we washed the pellet by adding 10 mL HEPES buffer solution and piped it out twice to remove Percoll. Before using the extracted chloroplast, we put the tubes upside down in the fridge for 1 h to get rid of the remained water or buffer solution from the chloroplast pellet. Extracted chloroplasts of various weight percent from 0 wt% to 5 wt% were gently mixed with the prepared polymer inks (with or without free NCO groups) using a magnetic stir bar for 30 min at 4°C in a dark environment to prevent the degradation of chloroplasts. Then, 2 wt% of photoinitiator (phenylbis(2,4,6-trimethylbenzoyl) phosphine oxide) was mixed with the polymer inks. The polymer was fully cured under white light from a white-light projector for 60 s.

To allow for the photosynthesis process, we placed the prepared chloroplast-embedded polymer samples in a white-light chamber (CL-1000 Ultraviolet Crosslinker with five UVP 34–0056–01 bulbs, light intensity 69.3W/m^2) and undergone various light illumination periods (0–4 h) and the respective darkness periods (same length of the illumination period). For example, the 15-min group went through 15-min light illumination and 15-min darkness. For the samples with various weight concentrations (0–5 wt%) of chloroplasts, they went through 4-h light illumination and 4-h darkness. After the illumination and darkness process, the samples were then uniaxially stretched until rupture with a strain rate of 0.05 s^{-1} with a mechanical tester (Instron, model 5942). The Young's modulus of each sample was calculated from the obtained tensile stress-strain curves (**Figs. 1de**).

To verify that photosynthesis can indeed assist the polymer strengthening, we study three sample groups for comparison: The experimental group includes polymer samples with free NCO groups and embedded chloroplasts, going through 4-h illumination and 4-h darkness, control 1 group that includes polymer samples with free NCO groups and embedded chloroplasts, going through 8-h darkness, and control 2 group that includes polymer samples with free NCO groups but without chloroplasts, going through 4-h light illumination and 4-h darkness. We compare the mechanical properties of three sample groups via uniaxial tensile tests (**Fig. 1d**). Compared to controls 1 and 2, the experimental group exhibits higher Young's modulus by a factor of 620% (**Fig. 1e**) and higher tensile strength by a factor of 350%.

In addition, we study the effects of two vital factors on the strengthening performance: concentration of embedded chloroplasts and light illumination period (**Fig. 2**). First, we employ various light illumination periods (white light intensity 0–69.3 W /m^2) to process the polymer samples with 5 wt% chloroplasts and free NCO groups. Tensile stress-strain curves show that Young's moduli increase with increasing illumination time within 0–2 h (**Fig. 2a-c**). Then, we investigate polymer samples with chloroplasts of various weight concentrations (0–5 wt%) and free NCO groups (processed with 4-h illumination and 4-h darkness). Tensile stress-strain curves show that Young's moduli increase with increasing chloroplast concentrations over 0–5 wt%, (**Figs. 2d-f**).

3. Theoretical model

In this section, we will establish a theoretical framework to understand the fundamental mechanics of photosynthesis-assisted polymer strengthening. The theory will explain the mechanisms of two processes: (1) Glucose is produced by the photosynthesis process within chloroplasts and then exported from the chloroplasts to the polymer matrix (**Section 3.1**), and (2) additional crosslinks are formed within the polymer network through the reaction between glucose and the NCO side groups (**Section 3.2**).

3.1. Part 1: glucose production and exportation

With the extracted chloroplasts embedded in the polymer matrix, the energy from light can trigger the photosynthesis process to produce glucose. The overall process of photosynthesis is shown in **Fig. 3a** (Gregory, 1977; Lawlor, 1993). During the daytime, chloroplasts first convert light energy to the energy-carrier molecules, and these molecules are simultaneously used to produce starch that is stored in the chloroplast. During the night, the accumulated starch is broken down as glucose and exported out of the chloroplast (**Fig. 3a**). In **Section 3.1.1**, we will model the conversion of light energy to chemical energy by considering a light-dependent reaction (**Fig. 3b**). In **Section 3.1.2**, we will model the production of starch by considering a photosynthetic carbon reduction (PCR) cycle or usually called the Calvin cycle (**Fig. 3c**). In **Section 3.1.3**, we will model the starch degradation and glucose export by using the Michaelis-Menten kinetic.

3.1.1. Kinetics of the light-dependent reaction

In the light-dependent reaction, the pigment chlorophyll can convert light energy to chemical energy in the form of adenosine triphosphate (ATP) and nicotinamide adenine dinucleotide phosphate (NADPH) (**Fig. 3b**), which are later used to produce glucose in the next stage of photosynthesis (Gregory, 1977; Lawlor, 1993). Photochemically, one molecule of the pigment chlorophyll absorbs
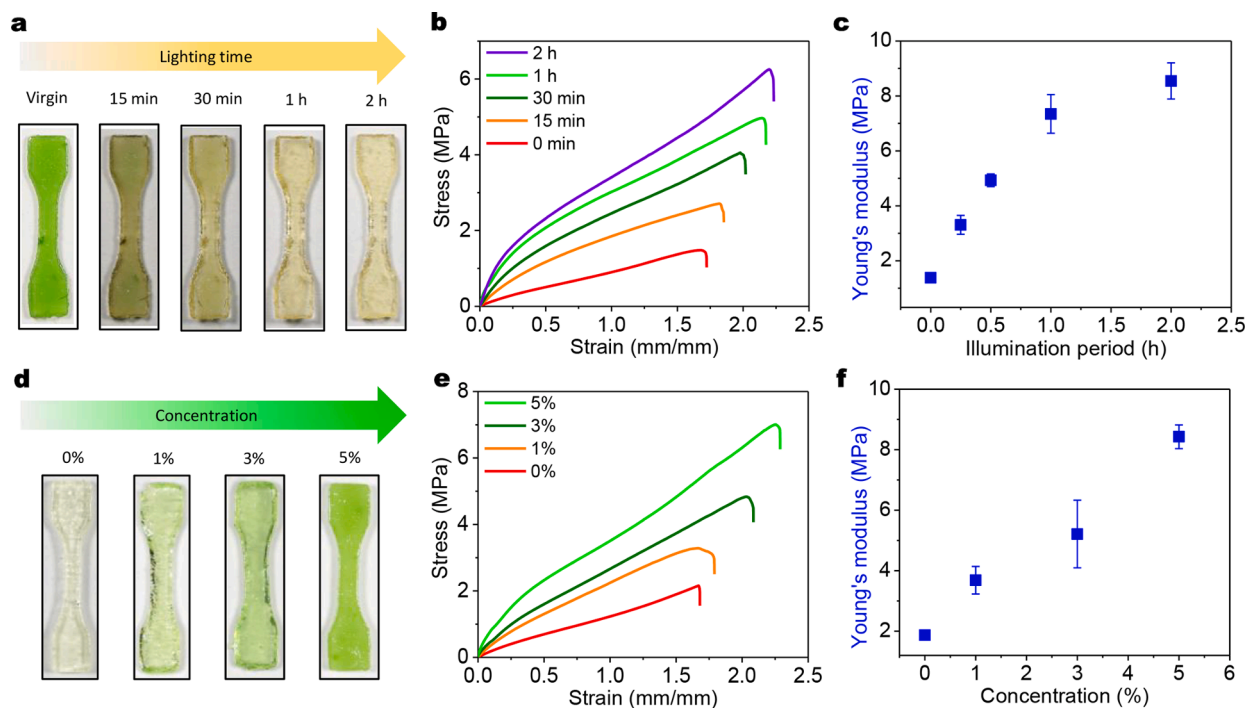

Fig. 2. (a) Samples with 5 wt% chloroplasts after the photosynthesis processes with various light illumination periods. (b) Uniaxial tensile stress-strain curves, (c) Young's moduli of samples with 5 wt% chloroplasts after the photosynthesis processes with various light illumination periods. Note that each light illumination period follows up with the same period of darkness period. (d) Samples with embedded chloroplasts of various weight concentrations. (e) Uniaxial tensile stress-strain curves, (f) Young's moduli of various weight concentrations samples undergo 4-h light illumination and 4-h darkness.
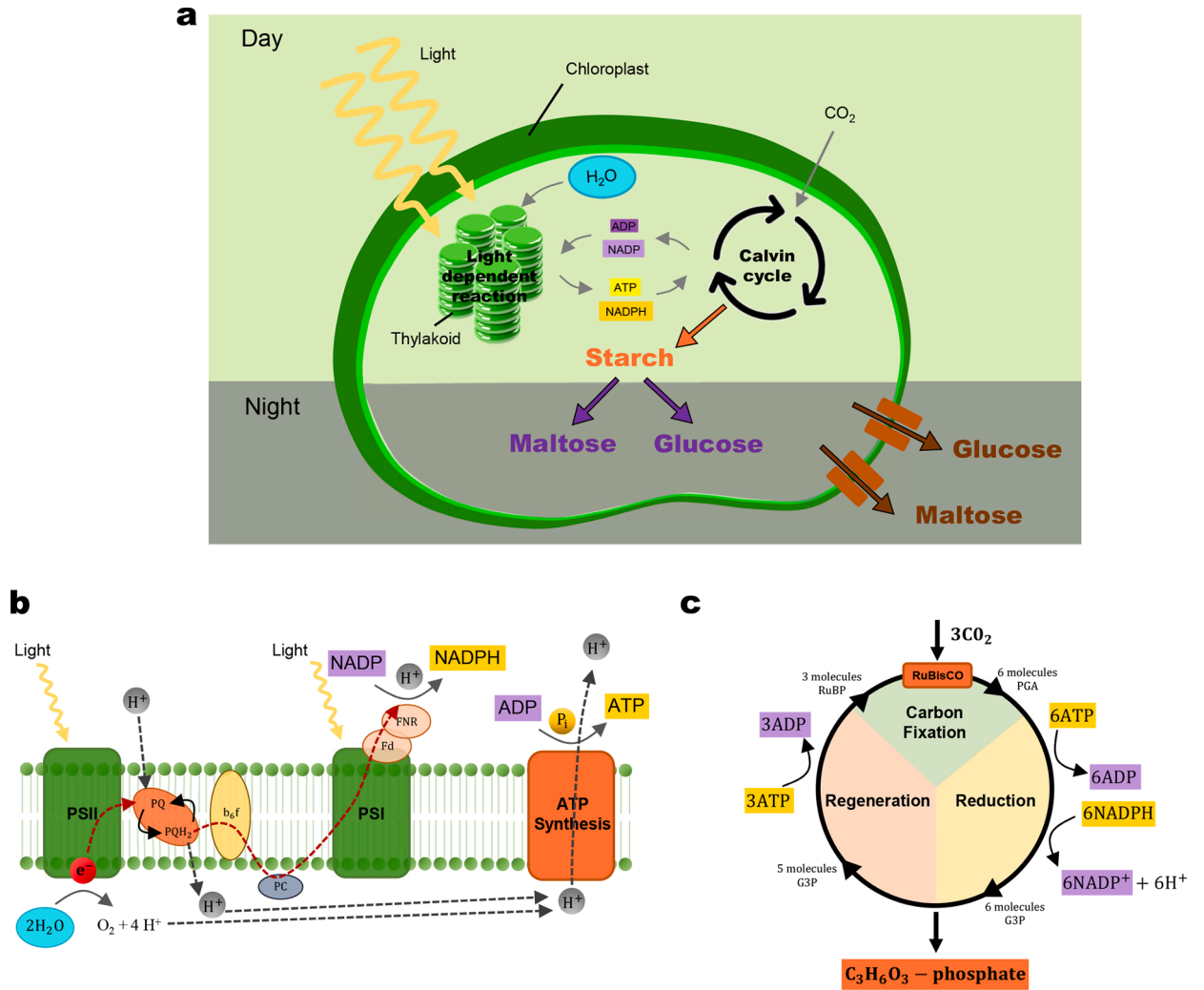
Fig. 3. Schematics of chloroplast to illustrate (a) overall photosynthesis process during day and night (b) light-dependent reaction (c) photosynthetic carbon reduction (PCR) cycle.

one photon and loses one electron (Von Caemmerer, 2000). This electron transfers to a modified form of chlorophyll called pheophytin, which passes the electron to a quinone molecule, starting the flow of electrons down to an electron transport chain that leads to the ultimate reduction of NADP to NADPH (**Fig. 3**b). In addition, this process creates a proton gradient (energy gradient) across the chloroplast membrane, which is used by photophosphorylation in the synthesis of ATP (**Fig. 3**b). The chlorophyll molecule ultimately regains the electron when a water molecule is split in a process called photolysis (or water splitting), which releases a dioxygen (O_2) molecule. The overall equation of the light-dependent reaction is written as

$$2\ H_2O + 2\ NADP^+ + 3\ ADP + 3\ Pi + 4\ h\nu\ \rightarrow 2\ NADPH + 2\ H^+ + 3\ ATP + O_2 \tag{1}$$
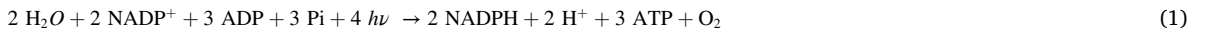
The net-reaction can be reduced as (Barber, 2017; Kok et al., 1970; Von Caemmerer, 2000; Yeung et al., 2015)

$$2\ H_2O + 4\ h\nu\ \rightarrow 4\ H^+ + O_2 \tag{2}$$

We consider a light source with an initial light intensity I_0 is illuminated on a polymer matrix with embedded chloroplasts. Due to the semitransparent color of the chloroplast-embedded sample, the light propagation will be attenuated through the polymer matrix, which can be described with the Beer-Lambert law (Long et al., 2011, 2009, 2013; Yu et al., 2019a),

$$\frac{\partial I(\mathbf{z})}{\partial \mathbf{z}} = -AI(z) \tag{3}$$

where the light illumination is along the z-axis, $I(z, t)$ is the light intensity at position **z** along the z-axis at time t, A is the absorption coefficient of the material. The light propagation direction is along a single axis (the z-axis); thus, we consider the light attenuation as a

1D problem (**Fig. 4**). The absorption coefficient can be estimated as (Vogelmann and Evans, 2002)

$$A = \alpha_1 \eta \tag{4}$$

where α_1 is the light absorption coefficient, and η is the mass concentration of the chloroplast within a unit volume of material (e.g., 0–5%, dimensionless). Here, we assume the polymer is incompressible, and thus the amount of chloroplast per unit volume will remain constant throughout the deformation.

With a constant initial light intensity I_0, the light intensity along the sample thickness direction (z-axis) can be written as (**Eq. (3)** and **Fig. 4**b),

$$I(z) = I_0 exp(-Az) \tag{5}$$

The chloroplasts embedded in the matrix absorb the photons via pigment chlorophyll and release electrons in the chloroplast. The governing equation of the absorbed photon concentration by the chlorophyll $C_p(z, t)$ can be written as (Long et al., 2011, 2009, 2013; Yu et al., 2019a; Zhao et al., 2015),

$$\frac{\partial C_p(z, t)}{\partial t} = \varepsilon_c \eta_M \alpha_2 \frac{1}{N_A} \frac{I(z)}{hc/\lambda} \tag{6}$$

where ε_c is the photosynthetic energy conversion efficiency of photon energy, η_M (mol/m^3) is the molar concentration of the chlorophyll, α_2 is the molar absorptivity of chlorophyll, $N_A = 6.02 \times 10^{23} \ mol^{-1}$ is the Avogadro number, $h = 6.63 \times 10^{-34} \ Js$ is the Plank constant, $c = 3 \times 10^8 \ ms^{-1}$ is the speed of light, and $\lambda = 550 \ nm$ is the mean wavelength of white light. Note that, η_M should be in a linear relationship with η, i.e., $\eta_M = \varphi \eta$, where $\varphi \approx 2.2 \times 10^{-3} mol/m^3$ (Von Caemmerer, 2000). In practice, chloroplasts do not convert all radiation energy into biomass energy, mainly due to the respiration requirements, reflection, and the need for optimal solar radiation levels. The overall photosynthetic efficiency is estimated between 3 and 6% of total photon energy (Bugbee and Salisbury, 1988; Zhu et al., 2010).

From **Eqs. (1)** and (2), the absorbed photon by the chlorophyll is used to create a proton gradient and then store the biomass energy in the chemical forms of ATP and NADPH. Since the formation of ATP and NADPH both require protons, to simplify the problem, we here consider the production of protons C_{H^+} as an irreversible chemical kinetic with photon energy to represent the formation of ATP and NADPH written as (Lei et al., 2007)

$$\frac{\partial C_{H^+}}{\partial t} = k_1 C_p(z, t) \tag{7}$$

where $k_1 \ (s^{-1})$ is the reaction rate to produce protons.

3.1.2. Photosynthetic carbon reduction (PCR) cycle

After the NADPH and ATP are generated from the light-dependent reaction, these energy-carrier molecules are simultaneously used to produce the glucose through the photosynthetic carbon reduction cycle (PCR cycle). In the PCR cycle, an enzyme called RuBisCO captures carbon dioxide from the atmosphere and uses the energies from NADPH and ATP to release hydrocarbon sugar (**Fig. 3**c).
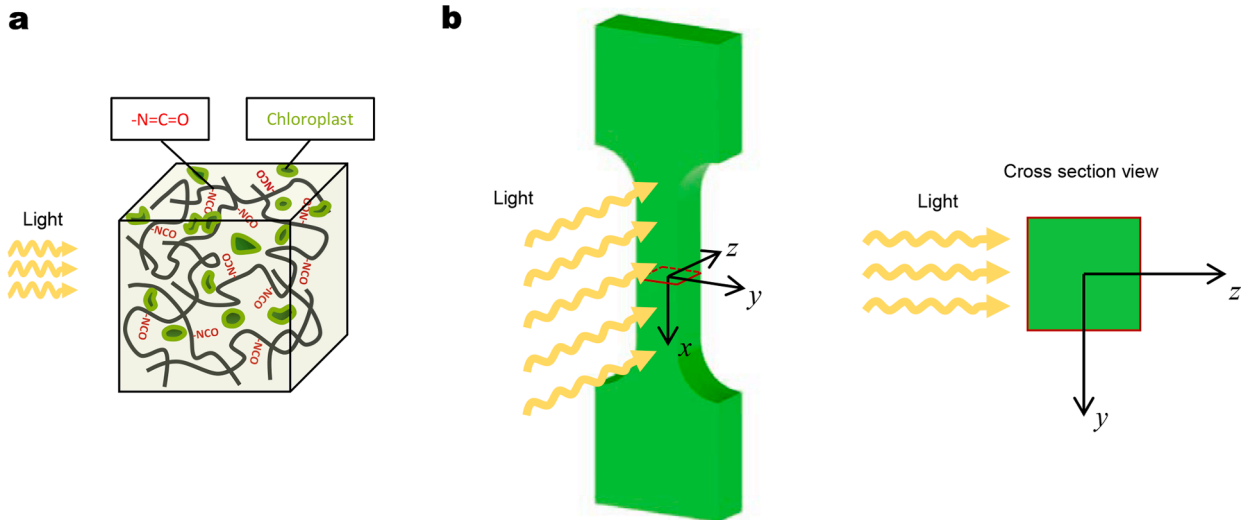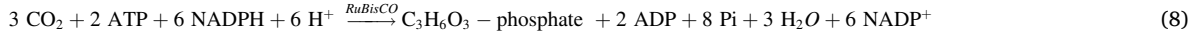

Fig. 4. (a) Schematics to illustrate the experiment procedure of light illuminate on the sample. (b) The global Cartesian coordinate system is constructed on the testing area. The light illumination direction is along the z-axis.

During the daytime, the released hydrocarbon sugar is temporarily stored in the chloroplast in the form of starch (Graf et al., 2010; Smith et al., 2005). The overall equation for PCR cycle is written as (Gregory, 1977; Lawlor, 1993; Von Caemmerer, 2000)

$$3 \text{ CO}_2 + 2 \text{ ATP} + 6 \text{ NADPH} + 6 \text{ H}^+ \xrightarrow{RuBisCO} \text{C}_3\text{H}_6\text{O}_3 - \text{phosphate} + 2 \text{ ADP} + 8 \text{ Pi} + 3 \text{ H}_2O + 6 \text{ NADP}^+ \tag{8}$$

Eq. (8) can be reduced by normalizing the coefficients as

$$\frac{1}{4} \text{ CO}_2 + \text{ H}^+ \xrightarrow{RuBisCO} \frac{1}{24} \text{ C}_6\text{H}_{12}\text{O}_6 + \frac{1}{4} \text{ H}_2\text{O} \tag{9}$$

The chemical kinetics between proton (H^+) and the produced $C_6H_{12}O_6$ in the form of starch during PCR cycle can be explained by the enzyme activity of RuBisCO following the Michaelis-Menten kinetics (Flamholz et al., 2019; Kubien et al., 2008; Zhu et al., 1998), written as,

$$\frac{\partial\left(C_{C_6H_{12}O_6}^{starch} \big/ 24\right)}{\partial t} = \frac{k_{cat1} C_{Rubisco} C_{H^+}}{C_{H^+} + k_{M1}} - k_t \left(\frac{C_{C_6H_{12}O_6}^{starch}}{24}\right) \tag{10}$$

where $C_{C_6H_{12}O_6}^{starch}$ is the concentration of the produced $C_6H_{12}O_6$ in the form of starch, k_{cat1} (s^{-1}) is the catalytic rate of RuBisCO, $C_{Rubisco}$ is the concentration of the enzyme RuBisCO, k_{M1} is the Michaelis constant of RuBisCO, and k_t is the termination rate of starch synthesis. We assume the gradually increased accumulation of starch in the chloroplast will result in termination of starch production, which has been found as a self-limiting process once the chloroplasts become saturated with transitory starch (Longland and Byrd, 2006). Note that the formation of starch typically requires a condensation reaction between a number of $C_6H_{12}O_6$ molecules, which kick out water molecules (Gregory, 1977; Lawlor, 1993; Von Caemmerer, 2000). However, the molar mass of starch is typically unknown; therefore, we only consider the amount of the smallest unit $C_6H_{12}O_6$ within the starch, but not directly consider the amount of the large starch molecule.

The production of starch during the photosynthesis process involves both the light-dependent reaction and the PCR cycle. The photon energy will first facilitate the production of biomass energies in the light-dependent reaction, and the enzyme will then facilitate the biomass energies to produce starch stored in the chloroplast (Smith et al., 2005). Therefore, these two processes are strongly coupled. Light can facilitate the production of biomass energy, and at the same time, the biomass energies are utilized by the enzyme to produce starch. This kinetic equation can effectively represent the overall photosynthesis chemical reaction, which is summarized as (Gregory, 1977; Lawlor, 1993; Von Caemmerer, 2000)

$$6 \text{ H}_2O + 6 \text{ CO}_2 \xrightarrow{12h\nu} C_6H_{12}O_6 + 6 \text{ O}_2 \tag{11}$$

3.1.3. Glucose exportation to matrix

During the night (darkness period), the accumulated starch in the chloroplast is first broken down into simple sugar such as maltose and glucose, which are then exported through the chloroplast membrane to the polymer matrix by glucose transporter (Fig. 3a) (Schafer et al., 1977; Servaites and Geiger, 2002). It is noteworthy that both maltose and glucose molecules have hydroxyl groups (OH), which can have a strong reaction with NCO groups within the initial polymer network. Since glucose is the simplest form of sugar and maltose is merely a form of multiple condensed glucose molecules, for simplicity, we here consider the product exported from the chloroplasts is glucose.

The breaking-down process of starch to form glucose molecules can be considered as a simple relationship with the darkness time (Chew et al., 2014; Graf et al., 2010; Lu et al., 2005), written as

$$\frac{dC_{gin}}{dt} = -\frac{dC_{C_6H_{12}O_6}^{starch}}{dt} = k_d C_{C_6H_{12}O_6}^{starch} \tag{12}$$

where C_{gin} is the concentration of glucose in the chloroplasts, k_d is the degradation rate of starch and $C_{C_6H_{12}O_6}^{starch}$ is the $C_6H_{12}O_6$ concentration in the form of starch.

The glucose molecules can be transported across the membrane of the chloroplast, assisted by the transportation enzyme (Nag et al., 2011). The enzyme-catalyzed transportation of glucose from chloroplast to material matrix can be explained with the Michaelis-Menten kinetics (Nag et al., 2011), written as

$$\frac{dN}{dt} = \frac{k_{cat2} C_{trans} C_{gin}}{C_{gin} + k_{M2}} \tag{13}$$

where dN/dt is the export rate of the glucose through the membrane transporter, k_{cat2} is the catalytic rate of glucose transport, C_{trans} is the concentration of transportation enzyme, and k_{M2} is the Michaelis constant of the enzyme. The incremental concentration of glucose per unit volume in the material matrix can thus be calculated as

$$\frac{dN}{V_{out}} = \frac{1}{V_{out}} \frac{k_{cat2} C_{trans} C_{gin}}{C_{gin} + k_{M2}} dt \tag{14}$$

where V_{out} is a unit volume of the material matrix. Therefore, the total concentration of glucose in a unit volume of the material matrix

at darkness time t_{dark} can be calculated as

$$C_{gout} = \frac{1}{V_{out}} \int_0^{t_{dark}} dN = \frac{1}{V_{out}} \int_0^{t_{dark}} \frac{k_{cat2} C_{trans} C_{gin}}{C_{gin} + k_{M2}} dt \tag{15}$$

Note that the chloroplast-produced glucose in the material matrix is a function of light intensity, light illuminating time, darkness time, and concentration of the embedded chloroplasts. We will further discuss the effects of these factors on the strengthening behaviors in **Section 4**.

3.2. Part 2: polymer strengthening by additional crosslinking

The initial polymer matrix is first crosslinked by the photoradical initiated addition reaction of the acrylate groups (**Fig. 5**a). Within this initial polymer network, NCO groups are active sites that can have a strong reaction with hydroxyl groups (OH) on the chloroplast-produced glucose to form urethane linkages (-NH—CO—O-). We here consider these newly formed urethane linkages as the new crosslinks additional to the acrylate-enabled crosslinks within the designed polymer matrix. In **Section 3.2.1**, we will first model the initial polymer network by considering a homogeneous chain length distribution network model; and in **Section 3.2.2**, we will model the strengthening of material by considering the formation of inhomogeneous chain lengths due to the additional crosslinks.

3.2.1. Initial polymer network

Before strengthening, the polymer network is assumed to feature a homogenous chain length. The chain length is described by the Kuhn length, denoted as N_0 and chain number per unit volume as n_0. The strain energy density of the polymer network can be written
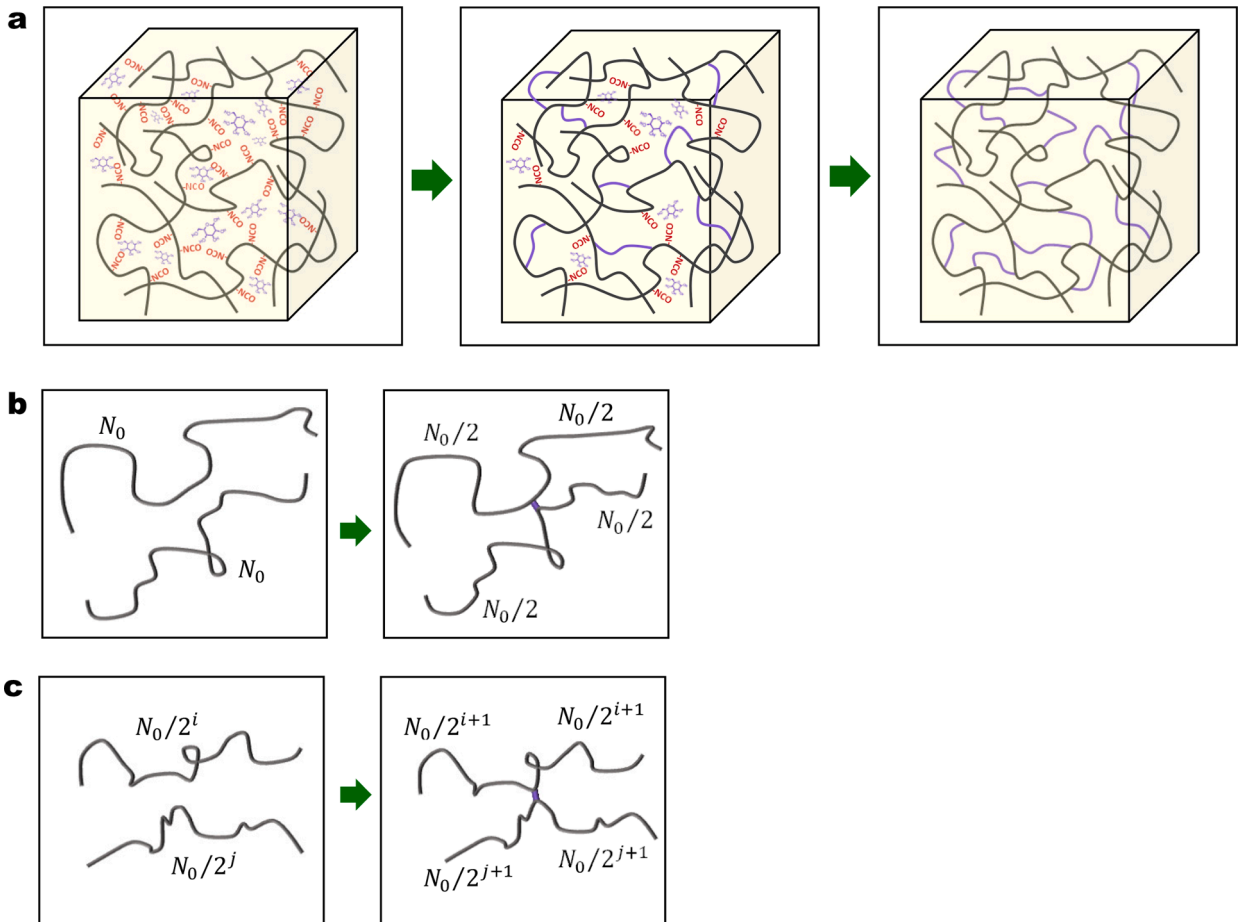

Fig. 5. (a) Schematics to show the formation of additional crosslinks through the reaction between the free NCO groups and the glucose. (b) Schematics to show the formation of one crosslink between two chains with the length of N_0. We assume each chain with the initial length of N_0 becomes two chains with the length of $N_0/2$. (c) Schematics to show the formation of one crosslink between a chain with the length of $N_0/2^i$ and a chain with the length of $N_0/2^j$. We assume the crosslink formed between a chain with the length of $N_0/2^i$ and a chain with the length of $N_0/2^j$ induces four chains with respective half lengths, where $i = 0, 1, 2\cdots$ and $j = 0, 1, 2\cdots$.

as (Arruda and Boyce, 1993; Treloar, 1975)

$$W_0 = n_0 k_B T N_0 \left(\frac{\beta_0}{tanh\beta_0} + ln \frac{\beta_0}{sinh\beta_0} \right) \tag{16}$$

where k_B is the Boltzmann constant, T is the temperature in Kelvin, and

$$\beta_0 = L^{-1} \left(\frac{\Lambda}{\sqrt{N_0}} \right) \tag{17}$$

where $L^{-1}()$ is the inverse Lagrange function and Λ is the chain stretch. Here, we follow an affine deformation assumption that the microscopic deformation at the polymer chain level affinely follows the macroscopic deformation at the material level in three principal directions; therefore, the chain stretch can be expressed as

$$\Lambda = \sqrt{\lambda_1^2 + \lambda_2^2 + \lambda_3^2} \tag{18}$$

This affine deformation assumption has been widely adopted for deriving the constitutive models for rubber-like materials, such as neoHookean model (Treloar, 1975) and Arruda-Boyce model (Arruda and Boyce, 1993). Note that Eq. (18) is slightly different from the corresponding relationship in the Arruda-Boyce model where the relationship is $\Lambda = \sqrt{(\lambda_1^2 + \lambda_2^2 + \lambda_3^2)/3}$. The chain stretch expressed in Eq. (18) is adopted for deriving the neoHookean model (Rubinstein and Colby, 2003; Treloar, 1975). We here adopt the network architecture from the neoHookean model but not the Arruda-Boyce network model, because a general network architecture that does not necessarily follow the eight-chain structure is more consistent with the network structure with additional crosslinks shown in Section 3.2.2.

If the material is incompressible, the Cauchy stresses in three principal directions can be written as

$$\begin{cases} \sigma_1 = \lambda_1 \dfrac{\partial W_0}{\partial \lambda_1} - P \\[2mm] \sigma_2 = \lambda_2 \dfrac{\partial W_0}{\partial \lambda_2} - P \\[2mm] \sigma_3 = \lambda_3 \dfrac{\partial W_0}{\partial \lambda_3} - P \end{cases} \tag{19}$$

where P is the hydrostatic pressure. Under uniaxially stretch with $\lambda_1 = \lambda$ and $\lambda_2 = \lambda_3 = \lambda^{-1/2}$, the Cauchy stresses σ_2 and σ_3 vanish. The Cauchy stress σ_1 can be formulated as

$$\sigma_1 = \lambda_1 \frac{\partial W_0}{\partial \lambda_1} - \lambda_2 \frac{\partial W_0}{\partial \lambda_2} \tag{20}$$

The corresponding nominal stress s_1 along λ_1 direction can be formulated as

$$s_1 = \frac{\sigma_1}{\lambda_1} = n_0 k_B T \sqrt{N_0} \ \frac{\lambda - \lambda^{-2}}{\sqrt{\lambda^2 + 2\lambda^{-1}}} L^{-1} \left(\sqrt{\frac{\lambda^2 + 2\lambda^{-1}}{N_0}} \right) \tag{21}$$

Through Eq. (21), we can obtain the uniaxial tensile stress-strain behaviors of polymer samples before strengthening. Only two fitting parameters (chain number density n_0 and polymer chain length N_0) are required.

3.2.2. Strengthening by forming additional crosslinks

Once the glucose is exported to the polymer matrix, the reactions between the free NCO groups and the OH groups on the glucose will form additional crosslinks (Fig. 5a). For forming a crosslink, one glucose molecule (with 5 OH groups) is only required to bridge two NCO groups. Thus, one glucose molecule is able to at best form 2.5 crosslinks within the network. The number of the introduced glucose molecules per unit volume is denoted as n_g and the formed additional crosslink number per unit volume is denoted as n_a. We should have $n_g \leq n_a \leq 2.5 n_g$.

As shown in Fig. 5b, two polymer chains with chain length N_0 will become four polymer chains with shorter lengths after introducing an additional crosslink. In a general case, these four polymer chains may have different chain lengths. Here, to capture the essential physics with a simple mathematic formulation, we assume these four polymer chains have the same chain length, as $N_0/2$. In a more general case shown in Fig. 5c, we assume the crosslink formed between a chain with length $N_0/2^i$ and a chain with length $N_0/2^j$ induces four chains with respective half lengths, where $i = 0, 1, 2 \cdots$ and $j = 0, 1, 2 \cdots$.

After introducing n_a additional crosslinks per unit volume, the initially homogeneous chain length (N_0) will become inhomogeneous, with a chain length distribution over length of $N_0, N_0/2, \ldots,$ and $N_0/2^m$, where $m \geq 1$. The value of m can be constrained by choosing the largest m to ensure

$$\frac{N_0}{2^m} \geq N_{min} \tag{22}$$

where N_{min} is the admissible smallest chain length.

To estimate the chain number of each type of chain length per unit volume, we treat the additional crosslinking process as m steps. In each step, a certain amount of additional crosslinking point is introduced. We employ two methods as follows.

3.2.2.1. Method 1: equal number of incremental crosslinking points. In method 1, we assume that probabilities of forming a crosslinking on the chain with length $N_0/2^i$ and the chain with length $N_0/2^j$ are equal, where $i = 0, 1, 2\cdots$ and $j = 0, 1, 2\cdots$. Under this assumption, the incremental additional crosslinking density for each step is equal, denoted as dn_a:

$$dn_a = \frac{n_a}{m} \tag{23}$$

In the following, we will go through each step to calculate the volume density of polymer chains with length $N_0/2^j$ and denote it as C_j, where $j = 0, 1, 2\cdots$. In step 1, some of the initial chains with length N_0 become shorter chains with length $N_0/2$ after adding dn_a crosslinking point if $2dn_a \leq n_0$. At the end of step 1, we have:

$$C_0 = n_0 - 2dn_a \tag{24}$$

$$C_1 = 4dn_a \tag{25}$$

In step 2, three possible routes to form the crosslinking: between two chains with length N_0, between two chains with length $N_0/2$, and between a chain with length N_0 and a chain with length $N_0/2$. The probabilities for partitioning chains with length N_0 and chains with length $N_0/2$ are equal. Therefore, at the end of step 2, we have:

$$C_0 = n_0 - 2dn_a - 2(dn_a/2) \tag{26a}$$

$$C_1 = 4dn_a + 4(dn_a/2) - 2(dn_a/2) \tag{26b}$$

$$C_2 = 4(dn_a/2) \tag{26c}$$

Similarly, at the end of step 3, we have:

$$C_0 = n_0 - 2dn_a - 2(dn_a/2) - 2(dn_a/3) \tag{27a}$$

$$C_1 = 4dn_a + 4(dn_a/2) - 2(dn_a/2) + 4(dn_a/3) - 2(dn_a/3) \tag{27b}$$

$$C_2 = 4(dn_a/2) + 4(dn_a/3) - 2(dn_a/3) \tag{27c}$$

$$C_3 = 4(dn_a/3) \tag{27d}$$

Eventually, at the end of step m, we have:

$$C_0 = n_0 - 2dn_a\left(1 + \frac{1}{2} + \frac{1}{3} + \cdots + \frac{1}{m}\right) \tag{28a}$$

$$C_1 = 2dn_a + 2dn_a\left(1 + \frac{1}{2} + \frac{1}{3} + \cdots + \frac{1}{m}\right) \tag{28b}$$

$$C_2 = 2(dn_a/2) + 2dn_a\left(\frac{1}{2} + \frac{1}{3} + \cdots + \frac{1}{m}\right) \tag{28c}$$

......

$$C_j = 2(dn_a/j) + 2dn_a\left(\frac{1}{j} + \frac{1}{j+1} + \cdots + \frac{1}{m}\right) \tag{28d}$$

......

$$C_m = 4(dn_a/m) \tag{28e}$$

The volume density of chains with length $N_0/2^j$ at the end of step m can be summarized as

$$C_j = \begin{cases} n_0 - \dfrac{2n_a}{m}\left(1 + \dfrac{1}{2} + \dfrac{1}{3} + \cdots + \dfrac{1}{m}\right), & j = 0 \\ \dfrac{2n_a}{m}\left(\dfrac{2}{j} + \dfrac{1}{j+1} + \cdots + \dfrac{1}{m}\right), & 1 \leq j \leq m-1 \ \ (if \ m \geq 2) \\ \dfrac{4n_a}{m^2}, & j = m \end{cases} \tag{29}$$

After strengthening, the polymer chain length is inhomogeneous with a chain length distribution over length of N_0, $N_0/2$, ..., and $N_0/2^m$, where $m \geq 1$. The chain length distribution is shown in **Eq. (29)**. We assume that under deformation, each polymer chain deform following an affine deformation assumption that the microscopic polymer chain deformation affinely follows the macroscopic deformation in three principal directions; thus, the chain stretch of the chain with length $N_0/2^j$ ($j = 0, 1, 2\cdots$) can be expressed as (Wang and Gao, 2016; Wang et al., 2017, 2015; Xin et al., 2019; Yu et al., 2020b, 2018, 2019a)

$$\Lambda_j = \sqrt{\lambda_1^2 + \lambda_2^2 + \lambda_3^2} \tag{30}$$

The strain energy of the whole polymer network per unit volume can be formulated as (Wang and Gao, 2016; Wang et al., 2017, 2015; Xin et al., 2019; Yu et al., 2020b, 2018, 2019a)

$$W_s = \sum_{j=0}^{m} \left[C_j k_B T \left(\frac{N_0}{2^j} \right) \left(\frac{\beta_j}{tanh\beta_j} + ln\frac{\beta_j}{sinh\beta_j} \right) \right] \tag{31}$$

$$\beta_j = L^{-1} \left(\frac{\Lambda_j}{\sqrt{N_0/2^j}} \right) \tag{32}$$

where the chain stretch Λ_j is given in **Eq. (30)**. Under uniaxial tension with $\lambda_1 = \lambda$ and $\lambda_2 = \lambda_3 = \lambda^{-1/2}$, the tensile nominal stress of the incompressible polymer after strengthening can be calculated as

$$s_{s1} = \sum_{j=0}^{m} \left[C_j k_B T \sqrt{N_0/2^j} \frac{\lambda - \lambda^{-2}}{\sqrt{\lambda^2 + 2\lambda^{-1}}} L^{-1} \left(\sqrt{\frac{\lambda^2 + 2\lambda^{-1}}{N_0/2^j}} \right) \right] \tag{33}$$

In method 1, there is a hidden requirement for the relationship between n_a and m. For example, if $m = 1$, the maximal possible crosslinking point density is $n_0/2$. This condition is to ensure the chain density of chains with length N_0 is not negative. For a certain m, the requirement of the possible crosslinking point density is

$$(m-1) \Big/ \left[2\left(1 + \frac{1}{2} + \frac{1}{3} + \cdots + \frac{1}{m-1} \right) \right] \langle n_a \Big/ n_0 \leq m \Big/ \left[2\left(1 + \frac{1}{2} + \frac{1}{3} + \cdots + \frac{1}{m} \right) \right] \tag{34}$$

3.2.2.2. Method 2: unequal number of incremental crosslinking points. In method 2, we assume that the probability of forming a crosslinking on the chain with length $N_0/2^i$ is higher than that of forming a crosslinking on the chain with length $N_0/2^j$ when $i < j$. In an extreme case, the crosslinking occurs first on the chain with length $N_0/2^i$, and then on the chain with length $N_0/2^{i+1}$. In other words, the crosslinking reaction on the longer chains always happens before the crosslinking reaction on the short chains. Following the assumption, we can naturally define the ith step as the step with the occurrence of the crosslinking reaction on the chain with length $N_0/2^{i-1}$. The process will move to the next step only when there are enough crosslinkers to consume all the chains with length $N_0/2^{i-1}$.

If the crosslinking reaction stops at step 1, there are only two types of chains: chains with length N_0 and $N_0/2$. Their volume densities can be calculated as

$$C_0 = n_0 - 2n_a \tag{35a}$$

$$C_1 = 4n_a \tag{35b}$$

The requirement is $0 < n_a/n_0 \leq 1/2$.

If the crosslinking reaction stops at step 2, there are only two types of chains: chains with length $N_0/2$ and $N_0/2^2$. Their volume densities can be calculated as

$$C_1 = 2n_0 - 2\left(n_a - \frac{n_0}{2} \right) = 3n_0 - 2n_a \tag{36a}$$

$$C_2 = 4\left(n_a - \frac{n_0}{2} \right) \tag{36b}$$

The requirement is $1/2 < n_a/n_0 \leq 3/2$.

If the crosslinking reaction stops at step m, at the end of step m, there are only two types of chains: chains with lengths $N_0/2^{m-1}$ and $N_0/2^m$. Their volume densities can be calculated as

$$C_{m-1} = 2^{m-1}n_0 - 2\left[n_a - \left(2^{m-2} - \frac{1}{2} \right)n_0 \right] = (2^m - 1)n_0 - 2n_a \tag{37a}$$

$$C_m = 4\left[n_a - \left(2^{m-2} - \frac{1}{2} \right)n_0 \right] = 4n_a - 4\left(2^{m-2} - \frac{1}{2} \right)n_0 \tag{37b}$$

The requirement is for the additional crosslink density to reach step m is

$$\frac{2^{m-1}-1}{2} < n_a \Big/ n_0 \leq \frac{2^m-1}{2} \tag{38}$$

After strengthening, the strain energy function can be formulated as (Wang and Gao, 2016; Wang et al., 2017, 2015; Xin et al., 2019; Yu et al., 2020b, 2018, 2019a)

$$W_s = \sum_{j=m-1}^{m} \left[C_j k_B T \left(\frac{N_0}{2^j}\right) \left(\frac{\beta_j}{\tanh\beta_j} + \ln\frac{\beta_j}{\sinh\beta_j}\right) \right] \tag{39}$$

$$\beta_j = L^{-1}\left(\frac{\Lambda_j}{\sqrt{N_0/2^j}}\right) \tag{40}$$

where the chain stretch Λ_j is given in Eq. (30) and C_j for $j = m-1$ and $j = m$ are given in Eq. (37). Under uniaxial tension with $\lambda_1 = \lambda$ and $\lambda_2 = \lambda_3 = \lambda^{-1/2}$, the nominal tensile stress of the incompressible polymer after strengthening can be calculated as

$$s_{s1} = \sum_{j=m-1}^{m} \left[C_j k_B T \sqrt{N_0/2^j} \; \frac{\lambda - \lambda^{-2}}{\sqrt{\lambda^2 + 2\lambda^{-1}}} L^{-1}\left(\sqrt{\frac{\lambda^2 + 2\lambda^{-1}}{N_0/2^j}}\right) \right] \tag{41}$$

4. Results

In this section, we first present the theoretical results calculated from the theory for glucose production and exportation (Section 4.1) and then from the theory for polymer strengthening by additional crosslinks (Section 4.2). In Section 4.3, we will integrate two parts of the theories and discuss the results for glucose-enabled additional crosslinks in the polymer matrix. By coupling the photosynthesis theory in Section 3.1 and the strengthening model in Section 3.2, we examine the effects of the illumination period, the

Table 1

Definition, value, and estimation source of the employed parameters. The estimation source is given for each parameter. I_0, η, and t are directly from experiments. N_0 and n_0 is estimated based on the stress-strain behaviors of the polymer.

Parameter	Definition	Fig. 6	Fig. 7,8	Fig. 9	Fig. 10, 11	Fig. 12	Fig. 13	Estimation source
I_0 ($J\ s^{-1}\ m^{-2}$)	Initial light intensity	69.3	N/A	N/A	69.3	69.3	0–69.3	Experimental data
α_1 (m^{-1})	Light absorption coefficient of the chloroplast	2000	N/A	N/A	2000	2000	2000	(Vogelmann and Evans, 2002)
η (%)	Mass concentration of the chloroplast	5	N/A	N/A	5	0–5	5	Experimental data
ε_c (%)	Photosynthetic energy conversion efficiency of photon energy	5	N/A	N/A	5	5	5	(Bugbee and Salisbury, 1988; Zhu et al., 2010)
α_2 ($m^2\ mol^{-1}$)	Molar absorptivity of chlorophyll	1×10^3	N/A	N/A	1×10^3	1×10^3	1×10^3	(Ergun et al., 2004)
k_1 (s^{-1})	Reaction rate to produce proton	1×10^4	N/A	N/A	1×10^4	1×10^4	1×10^4	(Lei et al., 2007)
k_{cat1} (s^{-1})	Catalytic rate of RuBisCO	3.13	N/A	N/A	3.13	3.13	3.13	(Flamholz et al., 2019; Kubien et al., 2008)
$C_{RubisCO}$ ($mol\ m^{-3}$)	Concentration of RuBisCO	0.008	N/A	N/A	0.008	0.008	0.008	(Kubien et al., 2008)
k_{M1} ($mol\ m^{-3}$)	Michaelis constant of RuBisCO	0.0021	N/A	N/A	0.0021	0.0021	0.0021	(Kubien et al., 2008)
k_t (s^{-1})	Termination rate of the starch synthesis	0.0004	N/A	N/A	0.0004	0.0004	0.0004	Fitting parameter
k_d (s^{-1})	Degradation rate of starch	0.003	N/A	N/A	0.003	0.003	0.003	(Lu et al., 2005)
k_{cat2} (s^{-1})	Catalytic rate of glucose transport	240.28	N/A	N/A	240.28	240.28	240.28	(Nag et al., 2011)
C_{trans} ($mol\ m^{-3}$)	Concentration of transportation enzyme	0.02	N/A	N/A	0.02	0.02	0.02	(Nag et al., 2011)
k_{M2} ($mol\ m^{-3}$)	Michaelis constant of enzyme	19.3	N/A	N/A	19.3	19.3	19.3	(Nag et al., 2011)
N_0	Initial chain length	N/A	100	40–2000	400	400	400	Chosen based on the material
n_0 (m^{-3})	Initial chain number density	N/A	4.5×10^{19}	4.5×10^{19}	4.5×10^{19}	4.5×10^{19}	4.5×10^{19}	Chosen based on the material
n_a/n_0	Normalized additional crosslink density	N/A	0–5	2.5	N/A	N/A	N/A	Chosen based on the material
t (h)	Illumination time	2	N/A	N/A	0–2	4	4	Experimental data

concentration of chloroplasts, and the light intensity on the strengthening performance. The theoretical results are compared with the experimental results. All used parameters are presented in **Table 1**.

4.1. Results of part 1 theory

In **Section 3.1**, a theoretical framework for the production and exportation of glucose was presented. During the illumination period, light intensity attenuates following the Beer-Lambert law (**Eq. (3)**). Considering a relatively thin sample ($H \sim 2\,mm$), we can calculate the mean light intensity across the thickness, written as,

$$\bar{I} \approx \frac{I_0}{2}[1 + exp(-AH)] \tag{42}$$

where H is the sample thickness. Note that in a real situation the light intensity is inhomogeneous across the thickness: more protons are produced at the locations closer to the light incident surface. It means that the glucose production and additional crosslinks will vary across the interface in the later process. Since the sample is thin (i.e., 2 mm), we here simplify the problem by considering an effectively homogeneous strengthening across the thickness. Using **Eq. (42)** and integrating **Eq. (7)**, we obtain the governing equation for the production of protons, expressed as,

$$\frac{\partial^2 C_{H^+}}{\partial t^2} = k_1 \varepsilon_c \eta_M \alpha_2 \frac{1}{N_a} \frac{\bar{I}}{hc/\lambda} \tag{43}$$

Coupling **Eqs. (43)** and (**10**), we can calculate the concentration of the produced $C_6H_{12}O_6$ in the form of starch ($C_{C_6H_{12}O_6}^{starch}$). A typical curve for the production of $C_6H_{12}O_6$ is shown in **Fig. 6a**. During the illumination period (2 h), the concentration of the produced $C_6H_{12}O_6$ in the form of starch increases over time and gradually reaches a plateau if the illumination time is long enough (**Fig. 6a**). The plateau is determined by the termination of the starch synthesis which is governed by the self-metabolism of the chloroplast.

During the darkness period, the starch begins to break down to form small glucose molecules which are then exported to the polymer matrix. Since the glucose exportation speed is dependent on the concentration of glucose within the chloroplast (**Eq. (13)**), the starch breaking-down and the glucose exportation are strongly coupled. Coupling **Eqs. (12)-(15)**, we can compute the evolution of the starch breaking-down and the glucose exportation, which are shown in **Figs. 6a and 6b**, respectively. As shown in **Figs. 6a**, the starch rapidly breaks down within 0.5 h. All of the produced $C_6H_{12}O_6$ molecules within chloroplasts are exported to the polymer matrix (as glucose molecules); thus, the concentration of the exported glucose increases over time and then reaches a plateau (**Fig. 6b**).
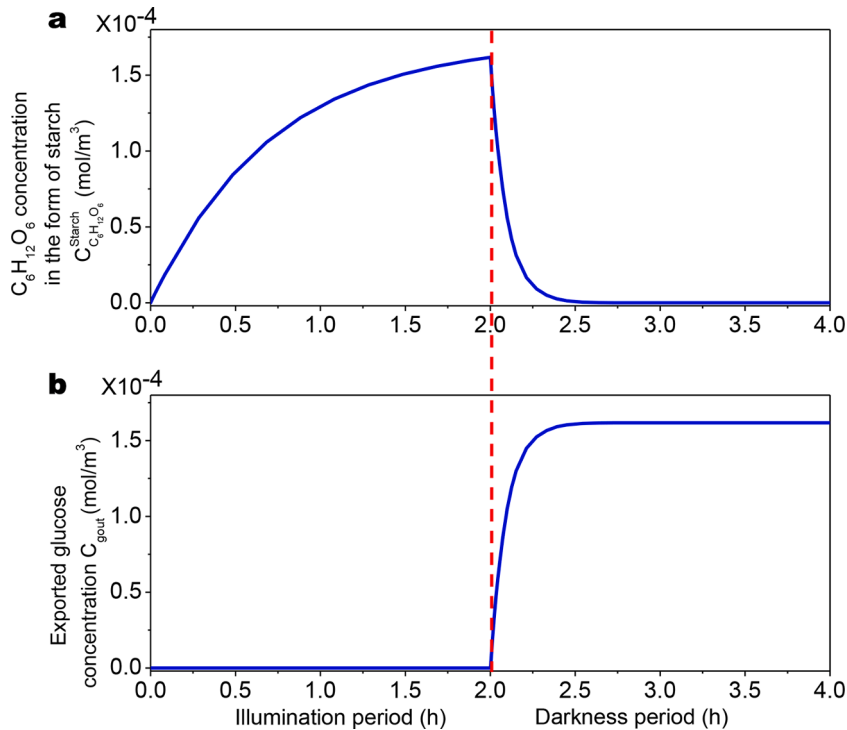

Fig. 6. (a) The evolution of $C_6H_{12}O_6$ concentration in the form of synthesized starch in the chloroplast and (b) the evolution of the concentration of the exported glucose in the matrix over the illumination period (2 h) and the darkness period (2 h).

4.2. Results of part 2 theory

We consider the polymer strengthening via forming additional crosslinks in the polymer matrix. To estimate the chain number of each type of chain length per unit volume, we employ two methods to calculate the amount of additional crosslinking in each crosslinking step in Section 3.2.2. As shown in Figs. 7ab and 7 cd, the polymer with initial chain length $N_0 = 100$ becomes stronger with increasing additional crosslinks for both method 1 and method 2. We here define the strengthening factor as the strengthened Young's modulus (within 10% strain region) normalized by the non-strengthened Young's modulus (Figs. 7bd).

When the additional crosslinks density is low (e.g. $n_a/n_0 \leq 1/2$), there is only one-step strengthening in either method 1 or method 2, i.e., $m = 1$ (Figs. 7ac, red and green lines, Figs. 7bd). The strengthening behavior and factor show the same results by both methods. When the additional crosslinks density is slightly larger than $1/2$ (e.g. $n_a/n_0 = 0.75$), the stress-strain curve and the strengthening factor calculated from method 1 and 2 are still similar (Figs. 7ac, blue line, Figs. 7bd). However, when n_a/n_0 increases to 1, the stress-strain curve and strengthening factor calculated from method 1 are much larger than those calculated from method 2 (Figs. 7ac, magenta line, Figs. 7bd). This is because the step number of method 1 reaches a larger number ($m = 5$) than the step number of method 2 ($m = 2$), corresponding to shorter chains in the polymer matrix according to Eqs. (29), (33), and (37).

To investigate the relationships between additional crosslinks density n_a/n_0 and the step number m, we calculate the step numbers for method 1 and 2 with n_a/n_0 from 0 to 5 (Fig. 8). When $n_a/n_0 \leq 1/2$, the step numbers m for methods 1 and 2 are both in the first step strengthening thus m values are the same. When n_a/n_0 increases to 5, the step number m for method 1 drastically increases to 45. However, the step number m is still 4 when $n_a/n_0 = 5$ for method 2.

To further investigate the effect of large step numbers on the polymer strengthening, we take a relatively large crosslinking number as an example (e.g., $n_a/n_0 = 2.5$). When $n_a/n_0 = 2.5$, the step number for method 1 increases to 21 (Fig. 8a), which means that the shortest chain length in the polymer matrix becomes $N_0/2^{21}$. This value should be constrained by the admissible smallest chain length N_{min} and the initial chain length N_0 of the polymer in Eq. (22). Considering the stress-strain curve shape of the studied polymer (Fig. 2), the initial chain length N_0 is estimated between 60 and 2000. $N_0/2^{21}$ becomes an invalid number for the chain length. Therefore, under such a situation that additional crosslink density is relatively large, method 1 cannot effectively model the strengthening behavior, and we can only employ method 2.

Using method 2, we study the effect of the initial chain length N_0 of the polymer on the strengthening effect (Fig. 9). When the initial chain length N_0 is very small (e.g. $N_0 = 40$), the polymer can be significantly strengthened. When the initial chain length N_0
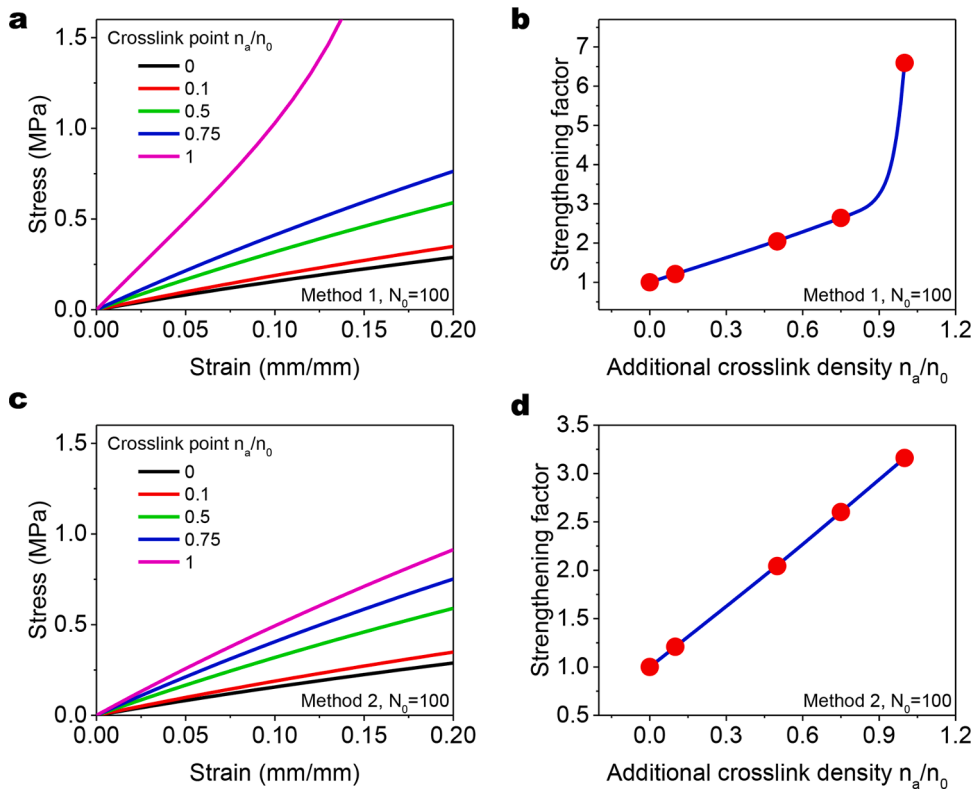

Fig. 7. Theoretical results for various normalized additional crosslink density n_a/n_0. (a) Nominal tensile stress-strain curves for method 1. (b) Strengthening factor in a function of the normalized additional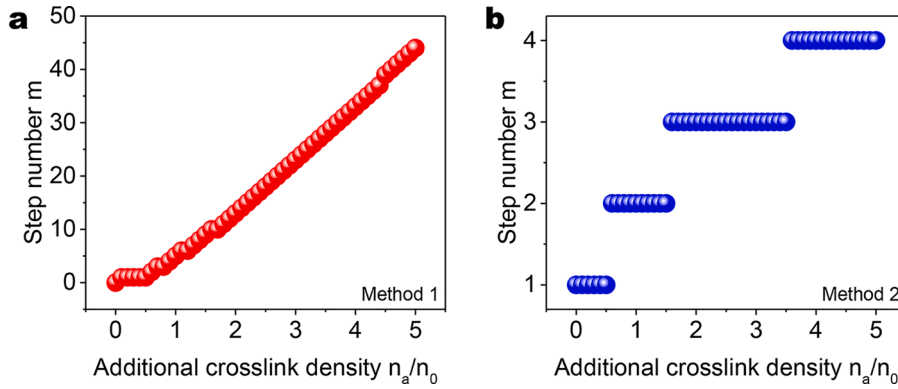 crosslink density for method 1. The strengthening factor is defined as the strengthened Young's modulus normalized by the unstrengthened Young's modulus. (c) Nominal tensile stress-strain curves for method 2. (d) Strengthening factor in a function of the normalized additional crosslink density for method 2.

Fig. 8. Relationships between the step number m and additional crosslink density n_a/n_0 for (a) method 1 and (b) method 2.

> 500, the strengthening factor reaches a plateau of around 6 (**Figs. 9ab**). When the initial chain length $60 \leq N_0 \leq 2000$, the strengthening factor varies from 6 to 7.9.

4.3. Results of the integrated theory

Integrating Part 1 and Part 2 theories, we can link the experimental conditions, such as light illumination and chloroplast concentration, to the resulting polymer strengthening. The connection between the Part 1 theory and Part 2 theory is the relationship between the concentration of the exported glucose and the concentration of additional crosslinks. We assume that all the exported glucose molecules are consumed by forming additional crosslinks, because the concentration of the NCO group is high enough. In addition, as a starting point, we assume one glucose molecule only bridges two NCO groups to form one additional crosslink, that is,

$$n_a = n_g = C_{gout}N_A \tag{44}$$

Eq. (44) constructs the connections between Part 1 theory and Part 2 theory. The concentration of the exported glucose calculated in Part 1 theory can be directly passed to Part 2 theory to determine the strengthening effect.

In the following sub-sections, we will first verify our theory for the glucose production/exportation with experimental results (**Section 4.3.1**), and then discuss the effects of the illumination period, the concentration of chloroplasts, and the light intensity on the polymer strengthening (**Sections 4.3.2-4**).

4.3.1. Verify the theory of glucose production via experiment

After the chloroplast-embedded polymer samples go through the photosynthesis process (illumination and darkness period), the glucose will be exported from the chloroplast to the polymer matrix. Since the photosynthesis-produced glucose is expected to consume free NCO groups to form additional crosslinks, the concentration reduction of free NCO groups can reveal the production and exportation of glucose. To indicate the concentration of free NCO groups within the polymer matrix, we employ a Fourier transform infrared (FTIR) spectrometer to measure the transmittance of the sample around 2260 cm^{-1} that is corresponding to the NCO bond stretching vibration (Yu et al., 2020a). We find an evident peak at 2260 cm^{-1} in the initial state of the sample (**Fig. 10a**). After the
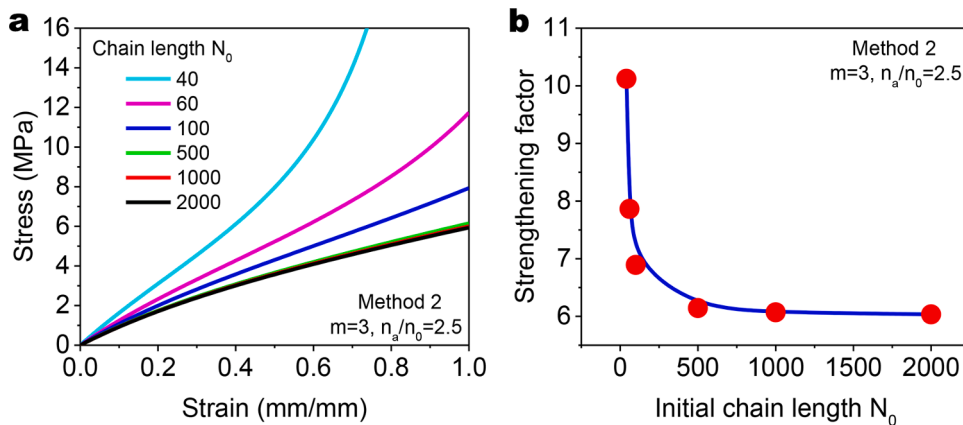

Fig. 9. Theoretical results for method 2 with $m = 3$ and $n_a/n_0 = 2.5$. (a) Nominal tensile stress-strain curves and (b) strengthening factor for various initial chain lengths N_0.

photosynthesis processes (illumination period and the corresponding darkness period of the same length), the peak at 2260 cm^{-1} drops, indicating the reduction of the NCO concentration. With increasing illumination periods (0–2 h), the peak height drops more. The initial concentration of NCO groups is denoted as C_0^{NCO}, and the concentration of NCO groups after the photosynthesis process with illumination period t_i us denoted as $C^{NCO}(t_i)$. To quantify the concentration reduction of NCO groups, we calculate the area under the FTIR peak ($S(t_i)$) and normalize the area with the initial peak area at 0 h (S_0) (**Fig. 10a**). We approximate the concentration ratio of NCO groups as

$$\frac{C^{NCO}(t_i)}{C_0^{NCO}} = \frac{S(t_i)}{S_0} \tag{45}$$

Since the consumed NCO groups have reacted with glucose molecules and one glucose molecule is assumed to consume two NCO groups, we obtain the exported glucose concentration as

$$C_{gout}(t_i) = 2C_0^{NCO}\left(1 - \frac{S(t_i)}{S_0}\right) \tag{46}$$

where $C_{gout}(t_i)$ is the concentration of the exported glucose after the illumination period of t_i and darkness period of t_i, and C_0^{NCO} can be calculated from the material recipe ($1.75 \times 10^{-4} mol/m^3$). **Fig. 10b** shows the relationship between the exported glucose concentration and the illumination period. The theoretically calculated concentration of the exported glucose agrees well with the experimental results obtained from **Eq. (46)**. As shown in **Fig. 10b**, the exported glucose concentration increases with the illumination period and gradually approaches a plateau when the illumination period is long enough.

4.3.2. Effect of the illumination period

With a longer illumination period, the photosynthesis process of chloroplasts is holding longer, thus leading to a higher concentration of produced $C_6H_{12}O_6$ stored in the form of starch at the end of the light-dependent process (**Fig. 11a**). According to **Eqs. (12)-(15)**, the stored starch in the chloroplast will degrade to glucose molecules and then transport to the material matrix, and the glucose molecules will serve as the additional crosslinks. With **Eq. (44)**, the amount of the exported glucose molecules can be passed to Part 2 theory to obtain the stress-strain behaviors of the strengthened polymers with various light illumination periods (**Fig. 11b**). Subsequently, Young's moduli of the strengthened polymers can be calculated within the strain range of 10% (**Fig. 11c**). As the illumination period increases, the concentration of the produced and exported glucose molecule increases, and the polymer thus becomes stiffer with a higher Young's modulus. As the illumination period further increases, the concentration of the exported glucose tends to approach a plateau; thus, Young's modulus of the strengthened polymer also tends to gradually reach a plateau (**Fig. 11c**). The theoretically calculated Young's moduli of the strengthened polymers for various illumination periods agree with the corresponding experimental results.

4.3.3. Effect of the chloroplast concentration

The chloroplast concentration greatly influences the polymer strengthening effect (**Figs. 2d-f**). The effect of the chloroplast concentration is displayed in two aspects. First, the color of chloroplast-embedded samples varies due to different concentrations of embedded chloroplasts (**Fig. 2d**). Due to the color difference, the light attenuation in the material matrix depends on the concentration of chloroplasts. This point can be modeled by **Eqs. (3)-(4)**, where the light absorption of the material depends on the concentration of chloroplast embedded in the polymer matrix. With increasing concentration of chloroplasts, the light intensity is attenuated more, and thus the mean light intensity cross the thickness $\bar{I}$ is lower (**Eq. (42)**). Second, a higher concentration of chloroplasts (η) leads to a higher concentration of chlorophyll (η_M in **Eq. (6)**), and thus more photon energy will be absorbed to produce the glucose. Since a
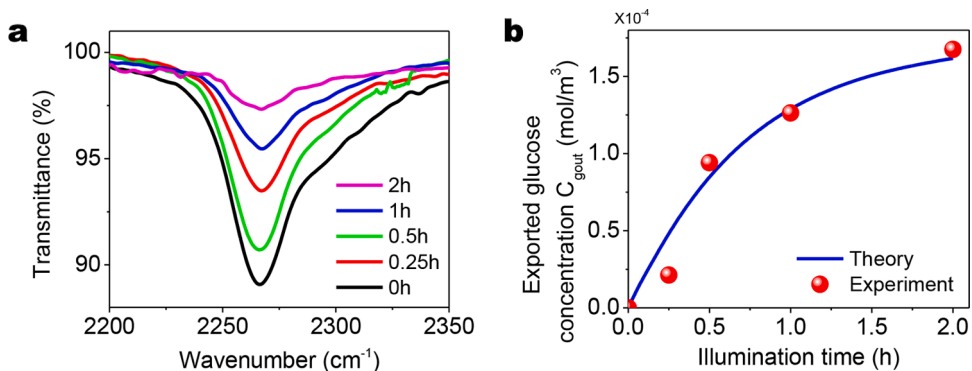

Fig. 10. (a) FTIR spectra of experimental group samples (with free NCO groups and embedded chloroplasts) with various light illumination periods. The zoom-in view of FTIR spectra in the range of 2200 cm^{-1} to 2350 cm^{-1} indicates the concentration of the free NCO groups. (b) Experimentally measured and theoretically calculated exported glucose concentration in a function of the illumination time. The experimental results are obtained using Eq. (46).
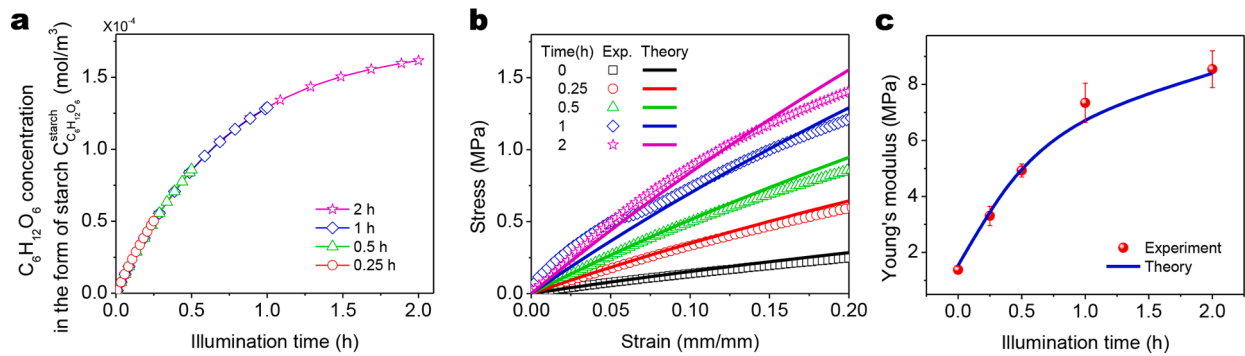
Fig. 11. (a) The theoretically calculated $C_6H_{12}O_6$ concentration in the form of starch for various light illumination periods. (b-c) Experimentally measured and theoretically calculated stress-strain curves and Young's moduli for various illumination periods. The Young's modulus is calculated from the stress-strain curve within 10% strain.

relatively thin sample ($H \sim 2\ mm$) is employed here, the effect of light attenuation is much smaller than the effect of light absorption. Overall, with increasing concentration of chloroplasts, more $C_6H_{12}O_6$ is synthesized during the light-dependent process (**Fig. 12a**) and then is exported as glucose molecules in the polymer matrix. The higher concentration of the exported glucose crosslinkers then leads to a stronger effect in the polymer strengthening. As shown in **Figs. 12ab**, as the concentration of chloroplasts increases from 0% to 5%, the resulting polymer matrix becomes stiffer with higher Young's modulus. The theoretically calculated stress-strain curves and Young's moduli agree with the respective experimental results (**Figs. 12bc**).

4.3.4. Effect of light intensity
Next, we study the effect of the applied light intensity (I_0) during the light-dependent process on the strengthening behavior. According to **Eqs. (3)**, (**6**), (**42**), **and** (**43**), the higher photon energy absorbed by the pigment chlorophyll induces more biomass energy converted to generate sugars. Theoretical results show that the plateau $C_6H_{12}O_6$ concentration stored in starch increases with increasing illuminating light intensity I_0 (**Fig. 13a**). In addition, according to **Eqs. (42) and** (**43**), such an increasing trend should be most linear. Such a linear trend is verified by the theoretically calculated relationship between Young's modulus of the strengthened polymer and the applied light intensity I_0 (**Fig. 13b**). The theoretically calculated Young's moduli agree well with the experimentally measured results (**Fig. 13b**).

Concluding remarks

In summary, we presented experiments and theories to study plant-inspired photosynthesis-assisted strengthening behaviors in a synthetic polymer. The strengthening mechanism relies on an additional crosslinking reaction between the photosynthesis-produced glucose and side groups within the polymer matrix. We develop a theoretical framework to explain glucose production and exportation, and the corresponding polymer strengthening by forming additional crosslinks. The theoretical framework can quantitatively explain the experimentally observed photosynthesis-assisted polymer strengthening under different experimental conditions, such as various illumination periods, concentrations of embedded chloroplasts, and light intensities.

The theoretical framework makes two significant advances in the field of solid mechanics. First, it, for the first time, proposes a simple and easy-to-implement theory to explain the polymer strengthening effect with additional crosslinks. This framework paves the way for the future mechanistic understanding of polymer network behaviors with incremental crosslinks, such as sequential crosslinking in double-network polymers/gels (Ducrot et al., 2014; Gong et al., 2003; Sun et al., 2012). Second, it, for the first time, proposes a theoretical framework to bridge the communication between the natural photosynthesis process and synthetic polymer networks. The communication between living photosynthesis and synthetic polymers may open doors for hybrid synthetic-living materials with both complex microstructures and biomimetic properties. The theoretical framework proposed in this paper may facilitate the mechanistic understanding of future hybrid synthetic-living materials.

Of course, the theoretical framework in this paper has been significantly simplified in multiple aspects. These aspects may forecast future research opportunities. For example, to capture the essence of the theory, we only focus our attention on the stress-strain behaviors within 20% strain and the corresponding Young's modulus (**Figs. 11–13**), but do not fully capture the stress-strain behaviors of the polymers until breaking during the tensile tests. As shown in **Fig. 2**, the stress-strain behaviors of the full strain regions until breaking may involve chain alternation and reorganization that may lead to softening or stiffening (Wang and Gao, 2016; Wang et al., 2015; Yu et al., 2018).

In addition, we do not consider the saturation of Young's modulus over various chloroplast concentrations and light intensities. In **Fig. 12**, we show that Young's modulus increases with increasing chloroplast concentration within 0–5%. With further increasing chloroplast concentration, we expect the modulus to saturate somewhere because chloroplasts that effectively behave like soft fillers may compromise the material stiffness. In **Fig. 13**, we show that Young's modulus increases linearly with the light intensity within $0\ -$ $69.3\ W/m^3$. With further increasing light intensity, we expect the modulus to saturate somewhere because strong light may damage
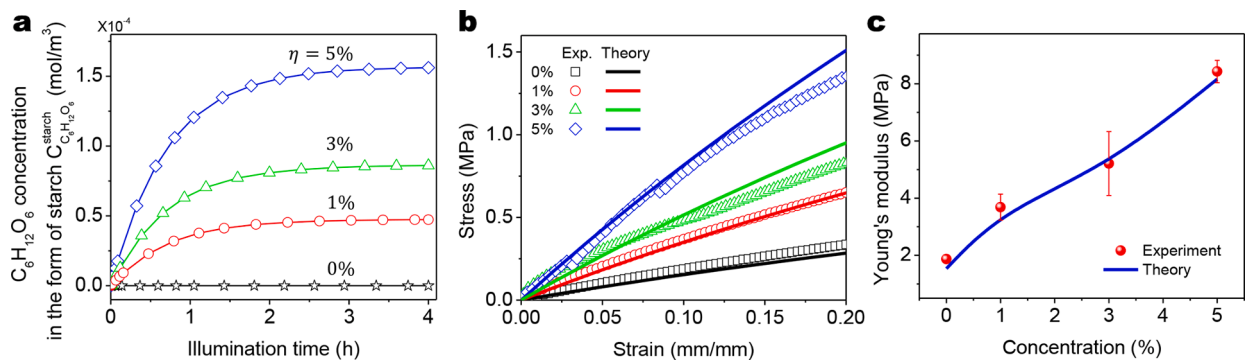
Fig. 12. (a) The theoretically calculated $C_6H_{12}O_6$ concentration in the form of starch for samples with various concentrations of embedded chloroplasts. (b-c) Experimentally measured and theoretically calculated stress-strain curves and Young's moduli for samples with various concentrations of embedded chloroplasts.
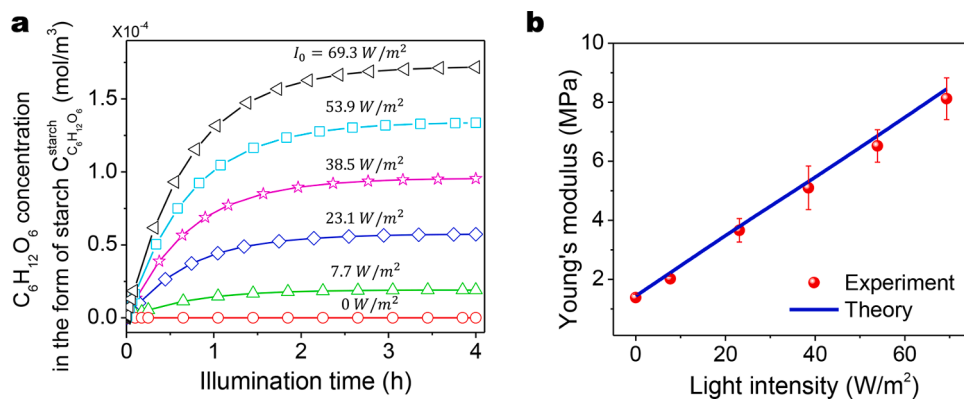

Fig. 13. (a) The theoretically calculated $C_6H_{12}O_6$ concentration in the form of starch for various applied light intensities. (b) Experimentally measured and theoretically calculated Young's moduli for various applied light intensities.

the chloroplasts and thus result in less exportation of glucose to the material matrix. Although these saturation behaviors may be interesting, this paper primarily focuses on modeling the effect of photosynthesis-produced glucose on the polymer strengthening, and thus does not include the saturation behavior in Figs. 12 and 13. Different from plants that chloroplast can be regenerated by their metabolisms, we chose moderate illumination periods, concentrations, and intensities to ensure the stability of the chloroplast activity in our material system (Walker et al., 1968). How to maintain the long-term living states of chloroplasts or even regenerate chloroplasts is very important for the future study.

As another example, in modeling the process of forming additional crosslinks, we consider that a crosslink would partition a chain into two halves with equal lengths. The realistic situation must follow a stochastic distribution. Besides, when considering the rule of forming additional crosslinks, we only consider two scenarios, namely the equal probability of forming additional crosslinks in chains with various lengths (method 1 in Section 3.2.2.1) and forming additional crosslinks in long chains (method 2 in Section 3.2.2.2). Only considering these two scenarios is for the sake of mathematical simplicity; however, the realistic situation should follow stochastic variations. We hope future models can include more careful considerations of the stochastic aspect.

Declaration of Competing Interest

The authors declare no competing interests.

References

Armon, S., Efrati, E., Kupferman, R., Sharon, E., 2011. Geometry and mechanics in the opening of chiral seed pods. Science 333, 1726–1730.

Arruda, E.M., Boyce, M.C., 1993. A three-dimensional constitutive model for the large stretch behavior of rubber elastic materials. J. Mech. Phys. Solids. 41, 389–412.

Barber, J., 2017. A mechanism for water splitting and oxygen production in photosynthesis. Nature Plants 3, 5.

Barthelemy, D., Caraglio, Y., 2007. Plant architecture: a dynamic, multilevel and comprehensive approach to plant form, structure and ontogeny. Ann. Bot. 99, 375–407.

Barthlott, W., Schimmel, T., Wiersch, S., Koch, K., Brede, M., Barczewski, M., Walheim, S., Weis, A., Kaltenmaier, A., Leder, A., Bohn, H.F., 2010. The salvinia paradox: superhydrophobic surfaces with hydrophilic pins for air retention under water. Adv. Mater. 22, 2325–2328.

Bartlett, N.W., Tolley, M.T., Overvelde, J.T.B., Weaver, J.C., Mosadegh, B., Bertoldi, K., Whitesides, G.M., Wood, R.J., 2015. A 3d-printed, functionally graded soft robot powered by combustion. Science 349, 161–165.

Bugbee, B.G., Salisbury, F.B., 1988. Exploring the limits of crop productivity .1. Photosynthetic efficiency of wheat in high irradiance environments. Plant Physiol. 88, 869–878.

Chew, Y.H., Wenden, B., Flis, A., Mengin, V., Taylor, J., Davey, C.L., Tindal, C., Thomas, H., Ougham, H.J., de Reffye, P., Stitt, M., Williams, M., Muetzelfeldt, R., Halliday, K.J., Millar, A.J., 2014. Multiscale digital arabidopsis predicts individual organ and whole-organism growth. Proc. Natl. Acad. Sci. U.S.A. 111, E4127–E4136.

Correa, D., Papadopoulou, A., Guberan, C., Jhaveri, N., Reichert, S., Menges, A., Tibbits, S., 2015. 3d-printed wood: programming hygroscopic material transformations. 3d Print. Addit. Manuf. 2, 106–116.

Del Dottore, E., Sadeghi, A., Mondini, A., Mattoli, V., Mazzolai, B., 2018. Toward growing robots: a historical evolution from cellular to plant-inspired robotics. Front. Robot. AI 5, 12.

Ducrot, E., Chen, Y., Bulters, M., Sijbesma, R.P., Creton, C., 2014. Toughening elastomers with sacrificial bonds and watching them break. Science 344, 186–189.

Ergun, E., Demirata, B., Gumus, G., Apak, R., 2004. Simultaneous determination of chlorophyll a and chlorophyll *b* by derivative spectrophotometry. Anal. Bioanal. Chem. 379, 803–811.

Farquhar, G.D., Caemmerer, S.V., Berry, J.A., 1980. A biochemical-model of photosynthetic co2 assimilation in leaves of c-3 species. Planta 149, 78–90.

Flamholz, A.I., Prywes, N., Moran, U., David, D., Bar-On, Y.M., Oltrogge, L.M., Alves, R., Savage, D., Milo, R., 2019. Revisiting trade-offs between rubisco kinetic parameters. Biochemistry 58, 3365–3376.

Gan, D.L., Xing, W.S., Jiang, L.L., Fang, J., Zhao, C.C., Ren, F.Z., Fang, L.M., Wang, K.F., Lu, X., 2019. Plant-inspired adhesive and tough hydrogel based on ag-lignin nanoparticles-triggered dynamic redox catechol chemistry. Nat. Commun. 10, 10.

Gong, J.P., Katsuyama, Y., Kurokawa, T., Osada, Y., 2003. Double-network hydrogels with extremely high mechanical strength. Adv. Mater. 15, 1155–1158.

Graf, A., Schlereth, A., Stitt, M., Smith, A.M., 2010. Circadian control of carbohydrate availability for growth in arabidopsis plants at night. Proc. Natl. Acad. Sci. U.S. A. 107, 9458–9463.

Gregory, R.P.F., 1977. Biochemistry of Photosynthesis. Wiley London.

Joly, D., Carpentier, R., 2011. Rapid isolation of intact chloroplasts from spinach leaves. In: Carpentier, R. (Ed.), Photosynthesis Research Protocols. Humana Press, Totowa, pp. 321–325.

Kok, B., Forbush, B., McGloin, M., 1970. Cooperation of charges in photosynthetic o2 evolution .1. A linear 4step mechanism. Photochem. Photobiol. 11, 457.

Kubien, D.S., Whitney, S.M., Moore, P.V., Jesson, L.K., 2008. The biochemistry of rubisco in flaveria. J. Exp. Bot. 59, 1767–1777.

Lawlor, D.W., 1993. Photosynthesis: molecular, physiological and environmental processes. Longman Sci. Tech.

Lei, Z., Su, M.Y., Chao, L., Liang, C., Hao, H., Xiao, W., Liu, X.Q., Fan, Y., Gao, F.Q., Hong, F.S., 2007. Effects of nanoanatase tio2 on photosynthesis of spinach chloroplasts under different light illumination. Biol. Trace Elem Res. 119, 68–76.

Li, S.Y., Wang, K.W., 2015a. Fluidic origami with embedded pressure dependent multi-stability: a plant inspired innovation. J. R. Soc., Interface 12.

Li, S.Y., Wang, K.W., 2015b. Fluidic origami: a plant-inspired adaptive structure with shape morphing and stiffness tuning. Smart Mater. Struct. 24.

Long, K.N., Scott, T.F., Dunn, M.L., Qi, H.J., 2011. Photo-induced deformation of active polymer films: single spot irradiation. Int. J. Solids Struct. 48, 2089–2101.

Long, K.N., Scott, T.F., Qi, H.J., Bowman, C.N., Dunn, M.L., 2009. Photomechanics of light-activated polymers. J. Mech. Phys. Solids 57, 1103–1121.

Long, R., Qi, H.J., Dunn, M.L., 2013. Thermodynamics and mechanics of photochemcially reacting polymers. J. Mech. Phys. Solids 61, 2212–2239.

Longland, A.C., Byrd, B.M., 2006. Pasture nonstructural carbohydrates and equine laminitis. J. Nutr. 136, 2099S–2102S.

Lu, Y., Gehan, J.P., Sharkey, T.D., 2005. Daylength and circadian effects on starch degradation and maltose metabolism. Plant Physiol. 138, 2280–2291.

Nag, A., Lunacek, M., Graf, P.A., Chang, C.H., 2011. Kinetic modeling and exploratory numerical simulation of chloroplastic starch degradation. BMC Syst. Biol. 5, 22.

Popper, Z.A., Michel, G., Herve, C., Domozych, D.S., Willats, W.G.T., Tuohy, M.G., Kloareg, B., Stengel, D.B., 2011. Evolution and diversity of plant cell walls: from algae to flowering plants. Annu. Rev. Plant Biol. 62 (62), 567.

Rubinstein, M., Colby, R.H., 2003. Polymer Physics. Oxford university press, New York.

Schafer, G., Heber, U., Heldt, H.W., 1977. Glucose-transport into spinach-chloroplasts. Plant Physiol. 60, 286–289.

Sehaqui, H., Salajkova, M., Zhou, Q., Berglund, L.A., 2010. Mechanical performance tailoring of tough ultra-high porosity foams prepared from cellulose i nanofiber suspensions. Soft Matter 6, 1824–1832.

Servaites, J.C., Geiger, D.R., 2002. Kinetic characteristics of chloroplast glucose transport. J. Exp. Bot. 53, 1581–1591.

Shah, D.U., Reynolds, T.P., Ramage, M.H., 2017. The strength of plants: theory and experimental methods to measure the mechanical properties of stems. J. Exp. Bot. 68, 4497–4516.

Smith, A.M., Zeeman, S.C., Smith, S.M., 2005. Starch degradation. Annu. Rev. Plant. Biol. 56, 73–98.

Sun, J.-.Y., Zhao, X., Illeperuma, W.R.K., Chaudhuri, O., Oh, K.H., Mooney, D.J., Vlassak, J.J., Suo, Z., 2012. Highly stretchable and tough hydrogels. NatureNature 489, 133–136.

Treloar, L.R.G., 1975. The Physics of Rubber Elasticity. Oxford University Press, USA.

Tricinci, O., Terencio, T., Mazzolai, B., Pugno, N.M., Greco, F., Mattoli, V., 2015. 3d micropatterned surface inspired by salvinia molesta via direct laser lithography. ACS Appl. Mater. Interfaces 7, 25560–25567.

Vogelmann, T.C., Evans, J.R., 2002. Profiles of light absorption and chlorophyll within spinach leaves from chlorophyll fluorescence. Plant Cell Environ. 25, 1313–1323.

Von Caemmerer, S., 2000. Biochemical Models of Leaf Photosynthesis. Csiro publishing.

Walker, D.A., Baldry, C.W., Cockburn, W., 1968. Photosynthesis by isolated chloroplasts simultaneous measurement of carbon assimilation and oxygen evolution. Plant Physiol. 43, 1419.

Wang, Q., Gao, Z., 2016. A constitutive model of nanocomposite hydrogels with nanoparticle crosslinkers. J. Mech. Phys. Solids 94, 127–147.

Wang, Q., Gao, Z., Yu, K., 2017. Interfacial self-healing of nanocomposite hydrogels: theory and experiment. J. Mech. Phys. Solids 109, 288–306.

Wang, Q., Gossweiler, G.R., Craig, S.L., Zhao, X., 2015. Mechanics of mechanochemically responsive elastomers. J. Mech. Phys. Solids 82, 320–344.

Xin, A., Zhang, R., Yu, K., Wang, Q., 2019. Mechanics of electrophoresis-induced reversible hydrogel adhesion. J. Mech. Phys. Solids 125, 1–21.

Yeung, L.Y., Ash, J.L., Young, E.D., 2015. Biological signatures in clumped isotopes of o-2. Science 348, 431–434.

Yu, K., Du, H., Xin, A., Lee, K.H., Feng, Z., Masri, S.F., Chen, Y., Huang, G., Wang, Q., 2020a. Healable, memorizable, and transformable lattice structures made of stiff polymers. NPG Asia Mater. 12, 26.

Yu, K., Feng, Z., Du, H., Xin, A., Lee, K.H., Li, K., Su, Y., Wang, Q., Fang, N.X., Daraio, C., 2021. Photosynthesis-assisted remodeling of three-dimensional printed structures. Proc. Natl. Acad. Sci. 118, 9.

Yu, K., Xin, A., Feng, Z., Lee, K.H., Wang, Q., 2020b. Mechanics of self-healing thermoplastic elastomers. J. Mech. Phys. Solids 137, 103831.

Yu, K., Xin, A., Wang, Q., 2018. Mechanics of self-healing polymer networks crosslinked by dynamic bonds. J. Mech. Phys. Solids 121, 409–431.

Yu, K., Xin, A., Wang, Q., 2019a. Mechanics of light-activated self-healing polymer networks. J. Mech. Phys. Solids 124, 643–662.

Yu, K.H., Xin, A., Du, H.X., Li, Y., Wang, Q.M., 2019b. Additive manufacturing of self-healing elastomers. Npg Asia Mater. 11, 11.

Zeiger, C., da Silva, I.C.R., Mail, M., Kavalenka, M.N., Barthlott, W., Holscher, H., 2016. Microstructures of superhydrophobic plant leaves - inspiration for efficient oil spill cleanup materials. Bioinspir. Biomim. 11, 9.

Zhao, Z.A., Mu, X.M., Sowan, N., Pei, Y.M., Bowman, C.N., Qi, H.J., Fang, D.N., 2015. Effects of oxygen on light activation in covalent adaptable network polymers. Soft Matter 11, 6134–6144.

Zhu, G.H., Jensen, R.G., Bohnert, H.J., Wildner, G.F., Schlitter, J., 1998. Dependence of catalysis and co2/o-2 specificity of rubisco on the carboxy-terminus of the large subunit at different temperatures. Photosyn. Res. 57, 71–79.

Zhu, X.G., Long, S.P., Ort, D.R., 2010. Improving photosynthetic efficiency for greater yield. Annu. Rev. Plant Biol. 61 (61), 235–261.

Zhu, X.G., Wang, Y., Ort, D.R., Long, S.P., 2013. E-photosynthesis: a comprehensive dynamic mechanistic model of c3 photosynthesis: from light capture to sucrose synthesis. Plant Cell Environ. 36, 1711–1727.